Steel and Composite Structures, *Vol. 26, No. 5 (2018) 621-634*
DOI: https://doi.org/10.12989/scs.2018.26.5.621

Seismic behaviour of gravity load designed flush end-plate joints

David Cassiano [1a], Mario D'Aniello [*2] and Carlos Rebelo [3b]

[1] *Constructure, Ltd, Unit D 15 Bell Yard Mews, London SE1 3TY, United Kingdom*
[2] *Department of Structures for Engineering and Architecture, University of Naples "Federico II", via Forno Vecchio, 36 – Napoli 80134, Italy*
[3] *ISISE, University of Coimbra, Polo II – R. Luís Reis Santos, 3030-788 Coimbra, Portugal*

(*Received June 12, 2017, Revised December 20, 2017, Accepted December 23, 2017*)

Abstract. Flush end-plate (FEP) beam-to-column joints are commonly used for gravity load resisting parts in steel multi-storey buildings. However, in seismic resisting structures FEP joints should also provide rotation capacity consistent with the global structural displacements. The current version of EN1993-1-8 recommends a criterion aiming at controlling the thickness of the end-plate in order to avoid brittle failure of the connection, which has been developed for monotonic loading conditions assuming elastic-perfectly plastic behaviour of the connection's components in line with the theory of the component method. Hence, contrary to the design philosophy of the hierarchy of resistances implemented in EN1998-1, the over strength and the hardening of the plastic components are not directly accounted for. In light of these considerations, this paper describes and discusses the results obtained from parametric finite element simulations aiming at investigating the moment-rotation response of FEP joints under cyclic actions. The influence of bolt diameter, thickness of end-plate, number of bolt rows and shape of beam profile on the joint response is discussed and design requirements are proposed to enhance the ductility of the joints.

Keywords: cyclic loading; beam-to-column joints; FEM; flush end-plate; seismic design

1. Introduction

Flush end-plate (FEP) beam-to-column joints are widely used and commonly considered as pinned joints in gravity load resisting frames. However, FEP joints typically behave as semi-rigid and partial strength, namely being characterized by moderate but non-negligible strength and stiffness. The current design rules and requirements (e.g., EN1993-1-8 (CEN 2005), AISC360-16 (AISC 2016c)) for FEP joints are mostly aimed at verifying the strength and the stiffness under monotonic bending and shear actions, but limited recommendations are available for seismic conditions. Even though FEP joints are not used for primary resisting structural systems, these joints should be able to guarantee ductility and rotation capacity compatible with the overall interstorey drift demand under seismic action without brittle failure.

In USA the common practice for bolted joints of primary seismic resisting systems is to adopt pre-qualified configurations (e.g., extended stiffened or unstiffened connections) in accordance with AISC358-16, which should guarantee a cyclic rotation capacity of 0.04 rad with residual strength no larger than $0.8M_p$ (being M_p the nominal plastic strength of the connected beam). However, no relevant pre-qualification rules are available for the joints used in gravity resisting frames such as FEP joints. In Europe, detailing rules for seismically prequalified connections are not currently available. EN1993-1-8 (CEN 2005) allows estimating solely the strength and the stiffness of FEP joints, without establishing rotation capacity under cyclic condition, even though a ductility criterion is provided to avoid T-stub mode 3 failure, by limiting end-plate thickness as respect to the bolt diameter.

Some studies were conducted in past decades to investigate the flexural behaviour of FEP joints. Srouji *et al.* (1983) and Bogsmiller and Murray (1995) developed prediction methods for the resistance using yield line theory. Boorse (1999) carried out experimental tests to assess the ductility under seismic loading, showing inelastic rotation capacity higher than 0.01 rad and also that wide bolt pitch configurations exhibit the higher rotation capacity with failure involving the fracture of both beam web to end-plate and beam flange to end-plate welds. Cyclic tests by Broderick and Thomson (2002) showed high ductility failure modes 1 and 2 and low ductility for mode 3 and that EN 1993-1-8 (CEN 2005) accurately predicted failure modes and bending strength, while overestimating stiffness by factors of 1.56 to 3.97. Tests by Aribert *et al.* (2004) showed that EN 1993-1-8 overestimates initial stiffness and that failure generally involves beam flange to end-plate welds that are prone to premature brittle failure. Tests on high strength connections with end-plates by Girão Coelho and Bijlaard (2007) showed similar results, namely that EC3 provided good agreement in terms of strength, while overestimating stiffness by 1.59 to 1.75 times. Experimental and numerical tests by Yu *et al.* (2011) have shown that thicker end-plates led to enhanced resistance coupled with limited ductility, with failure by a shear fracture of the end-plate close to the welds.

*Corresponding author, Ph.D., Assistant Professor,
E-mail: mdaniel@unina.it
[a] Ph.D., Structural Engineer
[b] Associate Professor, Ph.D.

ISSN: 1229-9367 (Print), 1598-6233 (Online)

To the best knowledge of the Authors, this review of the state of the art highlights the need to further investigation on the cyclic response of FEP joints, considering that FEP joints can be severely damaged during earthquakes. To this aim, a design rule is proposed to enhance the ductility of FEP joints. In addition, to verify the effectiveness of the proposed rule a numerical parametric study is conducted and the influence of the following parameters on joint response is investigated: bolt diameter, end-plate thickness, number of bolt rows and beam cross section. Numerical results are discussed in terms of moment-rotation response curves and compared to strength and stiffness limits from EN 1993-1-8 (CEN 2005) to identify the most effective details to maximize joint performance.

2. Design criteria

2.1 Eurocode criteria

According to the EN 1993-1-8 (CEN 2005) classification system, FEP joints are typically semi-rigid, implying that these elements should be explicitly modelled for structural analysis. This can be accomplished via the Components Method (CM), which provides an estimation of the initial stiffness and resistance. According to EN1993:1-8 (clause 6.4.2(2)), bolted end-plate joints have sufficient rotation capacity if their resistance is governed by either column flange or beam end-plate in bending without failure of bolts and welds. This condition is assumed as verified if the thickness of the plates of the connection satisfies the following condition

$$t \leq 0.36d \cdot \sqrt{f_{ub}/f_y} \quad (1)$$

The EN 1998-1 (CEN 2004) provides guidance regarding the design of primary and secondary seismic members. FEP joints are generally adopted for secondary gravity frame connections and are required to maintain load-carrying capacity when subjected to displacements induced by seismic action (clause 4.4.2). The design requirements for dissipative connections (clause 6.5.2) are based on capacity design principles. Furthermore, it is stated that dissipative semi-rigid and/or partial strength connections should have a rotation capacity consistent withglobal deformations (clause 6.6.4), which for DCH class structures should be larger than 35 mrad.

2.2 Revised ductility criterion

Joint ductility depends on the type of failure mode and on the plastic deformation capacity of the connection components. As shown by Fang *et al*. (2012, 2013), the strain hardening response of components significantly influence the ultimate response of flush end-plate joints.

In order to ensure ductility at local level, the resistance of bolts $F_{t,Rd}$ should be larger than the strength $F_{p,Rd}$ associated to failure mode type 1 at each bolt row, provided that the failure of welds is avoided. As highlighted by D'Aniello *et al*. (2017a), both the random variability of yield strength of plate material and its relevant strain hardening can be also accounted for as follows

$$F_{t,Rd} \geq \gamma \cdot F_{p,Rd} = \gamma_{ov} \cdot \gamma_{sh} \cdot F_{p,Rd} \quad (2)$$

where γ_{ov} is the random material overstrength factor (which it can be assumed equal to 1.25 as recommended by EN1998-1) and γ_{sh} is the strain hardening parameter, which can be assumed equal to $\gamma_{sh} = (f_y + f_u) / (2f_y)$ (being f_y the yield stress and f_u the ultimate stress of the steel plate) according to AISC (2016b). Re-arranging the inequality in Eq. (2), taking $\gamma_{M0} = 1.0$, $\gamma_{sh} = 1.20$ (as formerly adopted for extended stiffened end-plate bolted joints by D'Aniello *et al*. 2017a) and introducing the EN 1993-1-8 (CEN 2005) equations for yield line mechanism, the ductility criterion can be expressed as follows

$$t_{proposed} \leq \frac{0.42 \cdot d}{\sqrt{\gamma_{ov} \cdot \gamma_{sh}}} \cdot \sqrt{\frac{\gamma_{M0} \cdot f_{ub}}{\gamma_{M2} \cdot f_y}} \cong 0.30 \cdot d \cdot \sqrt{\frac{f_{ub}}{f_y}} \quad (3)$$

where f_{ub} is the ultimate bolt strength, f_y is the nominal plate yield strength and d is the bolt nominal diameter.

Hereinafter, the effectiveness of the ductility criterion for end-plate thickness given by Eq. (3) is investigated by means of parametric finite element simulations.

3. Parametric finite element analyses

The examined variables cover a representative set of realistic FEP joint configurations. Indeed, the beam-to-column assemblies are extracted from first storey spans of a set of steel moment resisting frames designed according to Eurocodes (Cassiano *et al*. 2016a) having span length equal to 6.0m and the column height equal to 3.5 m.

S355 steel grade is assumed for beams, columns and end-plates, while high-strength grade 10.9 steel is considered for bolts. Since the beam and the connection are the elements that mostly characterize the behaviour of FEP joints, in this study the column profile is kept constant, while beam and connection vary. The adopted column cross

Table 1 Definition of parametric variables

Parameter	Symbol	Examined values	Units
Number of bolt rows	R	{2 ; 4* }	[-]
Bolt diameter**	D	{16 ; 20 ; 24 }	[mm]
End-plate thickness	T	{8 ; 12 ; 16 ; 20 }	[mm]
Beam cross section	S	{IPE 220* ; IPE 360 ; HEA 320 ; HEA 500}	[-]

*4 bolt row configuration is not feasible for the case with IPE 220 profile. Indeed, in order to satisfy the minimum distances recommended by EN 1993-1-8 (CEN 2005), only in this case 3 bolt row configuration is adopted due to small depth of IPE200

**High strength bolts with grade 10.9 are adopted for all investigated diameters

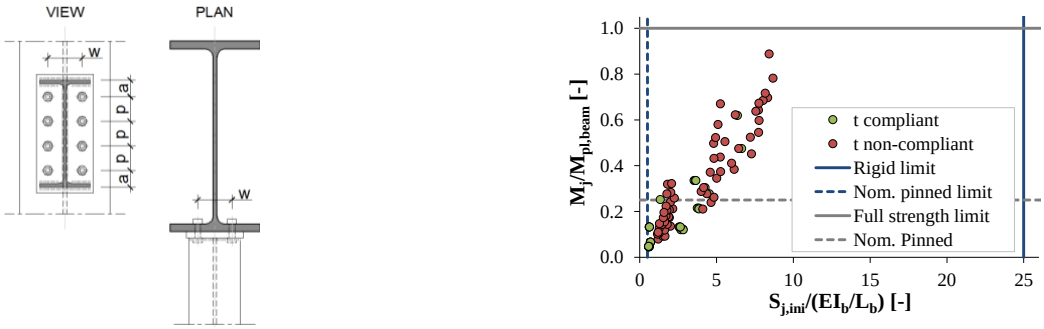

(a) Geometry (b) Joint normalised bending strength vs. stiffness distribution

Fig. 1 Investigated beam-to-column joints

Table 2 Details of examined flush end-plate joints

Beam section [-]	*p* (2 bolt rows) [mm]	*p* (4 bolt rows) [mm]	*a* [mm]	*w* [mm]
IPE 220	120	60*	50	114
IPE 360	248	83	56	114
HEA 320	189	63	61	168
HEA 500	348	83	71	168

*3 bolt rows

section (HEB 650) corresponds to the most commonly adopted in the set of reference frames. Both IPE and HEA sections were adopted, with depths ranging from 220 mm to 500 mm. The adopted parameters and the relevant variations are reported in Table 1. The following label code is used to identify each joint:

$$\mathbf{R}_{(\text{number of bolt rows})}\text{-}\mathbf{D}_{(\text{bolt diameter})}\text{-}\mathbf{T}_{(\text{thickness of end-plate})}\text{-}\mathbf{S}_{(\text{beam profile, either I or H})}$$

The typical geometry of the end-plate is presented in Fig. 1(a). Fig. 1(b) depicts the bending strength vs. stiffness distribution of the examined FEP joints, highlighting the joints compliant with the ductility criterion expressed by Eq. (3).

The geometrical features of the examined FEP joints are reported Table 2. In order to investigate the typical arrangement of gravity load design connection, the vertical pitch *p* is constant so as to equally space the bolt rows; the horizontal pitch *w* is assumed as the technological minimum distance, as conditioned by the fillet radius of the columns and the dimensions of bolts and corresponding washers. Fillet welds are considered for all joints. Full penetration welds are not considered because this type of details is not usually adopted for FEP joints. To try limitingthe brittle failure of fillet welds (Boorse 1999, Broderick and Thomson 2002, Yu *et al*. 2011), the throat depth of the fillet welds between the beam and the end-plate is assumed equal to 0.7 times the thickness of the thinnest connected plate.

3.1 Finite element modelling

Finite element models of FEP joints (see Fig. 2) are developed using ABAQUS (Dassault 2013). Both mechanical and geometrical nonlinearities are considered. C3D8R elements, i.e., reduced integration 8-node linear brick elements, are used with hourglass control and a minimum of three layers of finite elements along plate thickness to avoid shear locking problems. The structured meshing technique is assigned to obtain regular shapes for elements, especially for those elements discretizing rounded parts, e.g., bolt shanks, bolt head and nuts (Tartaglia and D'Aniello 2017, Tartaglia *et al*. 2018). The true stress-true strain relationship adopted for the analyses is taken from the average response of tensile coupon tests, using a combined isotropic/ kinematic hardening rule. The onset of plate fracture is evaluated a-posteriori through the Rupture Index, as described in Section 3.4. The evolution of residual resistance following fracture initiation is kept out of the scope of the present study. Fillet welds were modelled

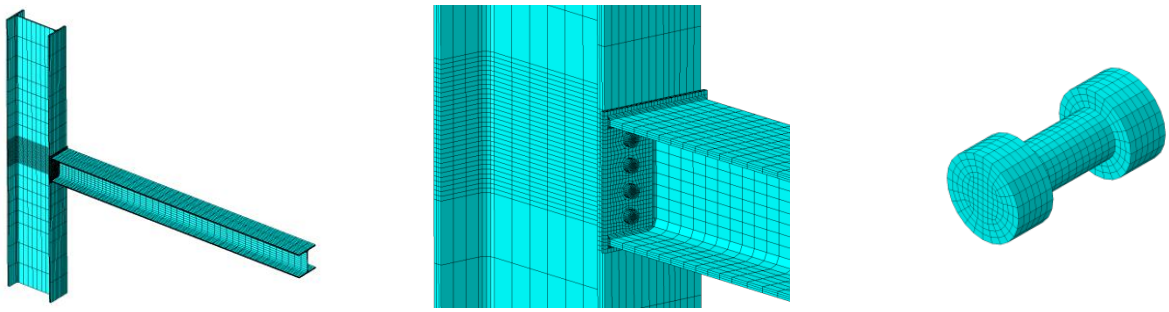

(a) Beam-to-column assembly (b) Joint (b) Bolt

Fig. 2 Finite element model of the R4-D20-T12-SH320 joint

according to their throat thickness assuming an elastic-perfectly plastic constitutive law, with f_y = 460 MPa, corresponding to an electrode grade A46 (ISO 2009). The bolts are modelled according to D'Aniello *et al*. (2017b), namely as a single part made of three partitioned zones, namely the shank, the head and the nut (see Fig. 2(c)). 3D solid finite element models with progressive damage are used, accounting for damage initiation, softening, crack initiation and progression. The undamaged material plasticity curve and the equivalent plastic strain at damage onset curve as a function of triaxial stress state are taken in line with Pavlovic *et al*. (2015). Contacts are modelled using hard contact law with tangent "Coulomb friction" (slip coefficient equal to 0.3) to simulate the interactions between (i) the end-plate and column flange; (ii) the bolt nuts and the surfaces of end-plate and column flange; and (iii) the bolt shanks and the holes of both end-plate and column flange.

Boundary conditions are applied to reference points tied to the cross sections surfaces at both ends of the columns and at the beam tip. The 3 translational degrees of freedom (DOFs) and the torsional DOFs are restrained at the lower end of the column; the vertical translational DOF is released at its top end to allow column shortening. For the beam tip section, all DOFs are restrained except for bending rotation about the strong axis.

Two levels of axial force in the column are considered: (i) zero axial force; (ii) 30% of the plastic strength of the column (higher than the maximum axial force from Cassiano *et al*. 2016). However, the obtained results showed that axial force in the column within the examined range has negligible influence on the joint response, in line with experimental results on joints under column loss by Kuhlmann *et al*. (2009). Therefore, this parameter is not discussed hereinafter.

Both monotonic and cyclic loading are considered. In both cases the numerical analyses are performed in two steps: (i) application of the EC3-compliant tightening force to the bolts; (ii) imposing vertical displacements to the beam end according to the AISC 341-16 (AISC 2016a) cyclic loading protocol. It should be noted that according to AISC 341-16 the connections can be seismically qualified if they are capable of withstanding interstorey drift angles of 40 mrad, whereas the EN 1998-1 (CEN 2004) states that for dissipative semi-rigid and/or partial strength joints the rotation capacity of the plastic hinge should not be less than 35 mrad for high ductile structures. In order to examine the response of the joints under both criteria, the loading protocol was applied up to an interstorey drift angle θ = 40 mrad.

3.2 Validation of the FE model

The assumptions for the finite element models are validated against the results of experimental tests carried out by Broderick and Thomson (2002). Fig. 3(a) shows the comparison between the FE prediction and the experimental response curve of the specimen EP2 tested by Broderick and Thomson (2002). The EP2 beam-to-column joint was characterized by a beam UB 254×102×22 and a column UC 203×203×86, both profiles were made of S275 steel grade. The distance between the point of application of the load and the end-plate was set equal to 750 mm. The width and depth of the flush end-plate were set equal to 200 mm and 275 mm, respectively, while its thickness was equal to 12 mm with only two bolt rows, each of them located at 60 mm from the beam flange. Two bolts M20 grade 8.8 were used per row, and the bolt gauge width was equal to 90 mm.

Since the ultimate resistance and ductility of the bolts largely influence the system ductility (Broderick and Thomson 2002, Aribert *et al*. 2004) and the accuracy of FE models, the modelling assumptions of bolts are also validated on the basis of experimental results on high strength bolts performed by D'Aniello *et al*. (2016). Also in this case the FE predictions accurately reproduce the experimental response, as shown in Fig. 3(b).

3.3 Strain rate effect

The influence of strain rate on the constitutive law of steel under seismic actions has been the subject of several studies. Dusicka *et al*. (2007) showed that strain rates ranging from 0.001s^{-1} (quasi-static) to 0.1s^{-1} lead to negligible differences in the cyclic response of steel coupon specimens up to axial strains equal to 4%. Gioncu *et al*. (2014) showed that the increase in yield strength is

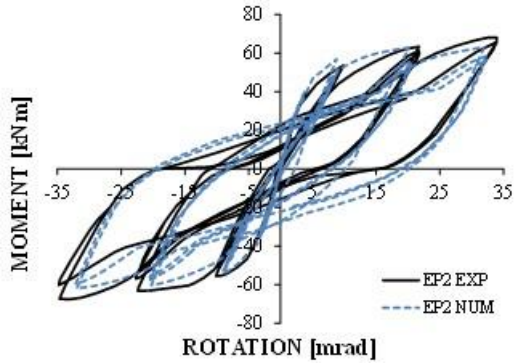

(a) Response of calibrated FE model of the EP2 joint by Broderick and Thomson (2002) vs experimental curve

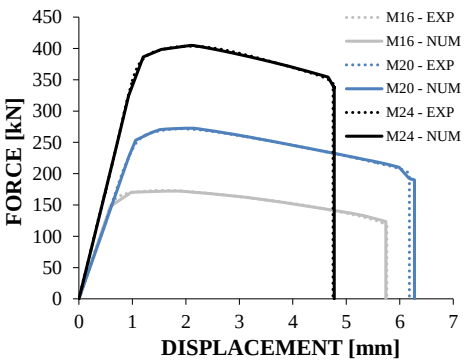

(b) Response of calibrated FE model of bolts vs experimental curves given by D'Aniello *et al*. (2016)

Fig. 3 Experimental vs. simulated response: (a) the joint; and (b) the bolt

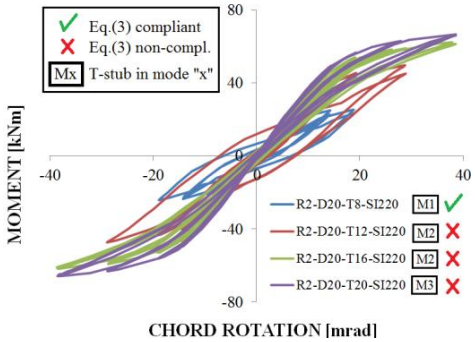

(a) Moment-chord rotation response for different values of end-plate thickness

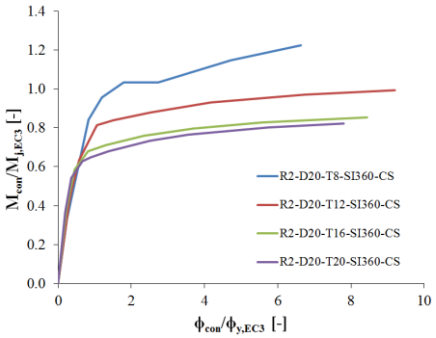

(b) Moment-rotation backbone curves normalised to EN 1993-1-8 joint strength for R2-D20-SI360 joints

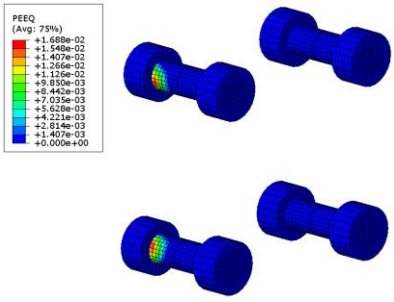

(c) Bolt plasticisation for the t = 20 mm end-plate at the end of the cyclic loading protocol

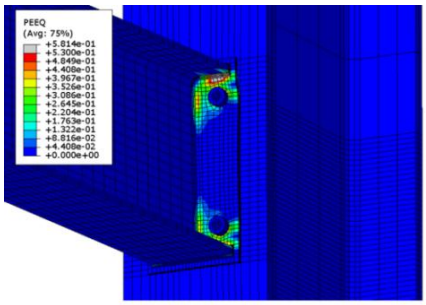

(d) PEEQ at fracture initiation – R2-D20-T8 -SI360 joint

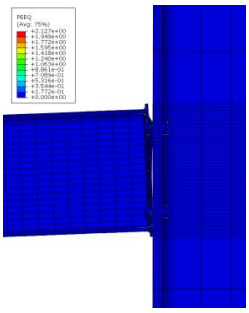

(e) Detail of the gap rotation for the R2-D20-T8-SI360 joint

Fig. 4 Cyclic response of the R2-D20 joints

negligible for strain rates in the range 0.1s^{-1} to 100s^{-1} (the latter representative of near-field earthquakes). Another experimental study carried out by Lamarche and Tremblay (2011) showed the ratio between the dynamic and static yield strength to be lower than 1.07 for strain rates equal to 0.5s^{-1}. In the light of the results provided by these studies, the enhancement effect induced by strain rates under seismic actions is conservatively disregarded in the analyses shown hereinafter.

3.4 Plate ductile fracture initiation

The plate ductile fracture initiation is monitored using the plastic equivalent strain index *PEEQ* determined from Rupture Index *RI* values from literature, hence allowing to investigate the limit state after which a significant drop in resistance occurs. The *RI* is defined as the ratio between the *PEEQ* and the ductile fracture strain ε_f, multiplied by the material constant a (El-Tawil *et al*. 1999), as follows

$$RI = a\frac{PEEQ}{\varepsilon_f} = \frac{PEEQ}{exp(-1.5T)} \tag{4}$$

where the *PEEQ* value that causes fracture can be obtained for a given stress triaxiality condition. The strain at ductile fracture initiation according to Hancock and Mackenzie (1976) is given by

$$\varepsilon_f = a \cdot exp\left(-1.5\frac{\sigma_H}{\sigma_{eq}}\right) = a \cdot exp(-1.5T) \tag{5}$$

where ε_f is the ductile failure strain, a is the material constant, σ_H is the hydrostatic stress defined in Eq. (8), σ_{eq} is the Von Mises stress defined in Eq. (9) and T is the stress triaxiality given by the ratio between σ_H and σ_{eq}.

$$\sigma_H = \frac{\sigma_{xx} + \sigma_{yy} + \sigma_{zz}}{3} \tag{6}$$

$$\sigma_{eq} = \sqrt{\frac{\left(\sigma_{xx} - \sigma_{yy}\right)^2 + \left(\sigma_{yy} - \sigma_{zz}\right)^2 + (\sigma_{zz} - \sigma_{xx})^2 + 6\left(\tau_{xy}{}^2 + \tau_{yz}{}^2 + \tau_{zx}{}^2\right)}{2}} \tag{7}$$

This procedure enables to predict the fracture initiation based on experimental results (El-Tawil *et al*. 1999). A numerical study by Zangouie and Deylami (2013) on the seismic performance of end-plate connections showed anaverage *PEEQ* = 0.71 at crack initiation, associated to a coefficient of variation *CoV* = 0.25, for beam flange thicknesses ranging from 9 mm to 20 mm and for 40 mrad drift. Myers *et al*. (2010) predicted fracture using the Stress Modified Critical Strain (SMCS) (Hancock and Mackenzie 1976) by verifying when the equivalent plastic strain at any point exceeds a critical value, according to the following expression

$$\bar{\varepsilon}_p > \bar{\varepsilon}_{p,critical} = \alpha \cdot exp(-1.5T) \tag{8}$$

Once the material-dependent toughness parameter α is determined, Eq. (8) can be used to predict the fracture

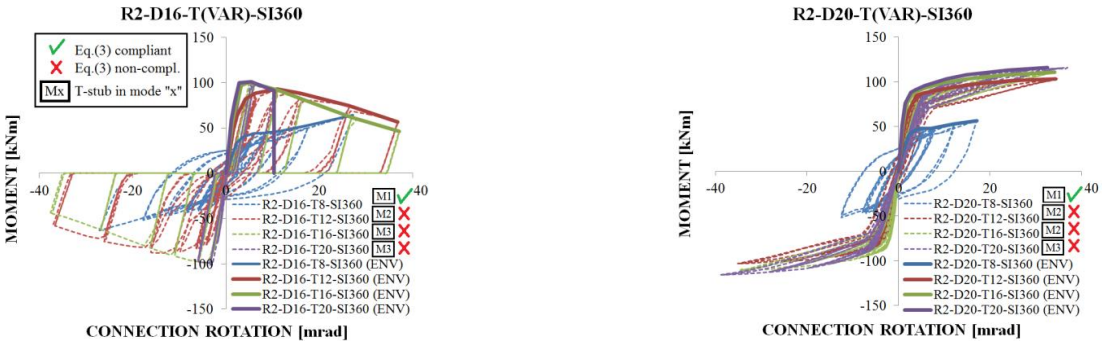

(a) M16 bolt assemblies (b) M20 bolt assemblies

Fig. 5 Effect of end-plate thickness on R2-SI360 joints: M-$\theta_{connection}$ and cyclic envelope curves

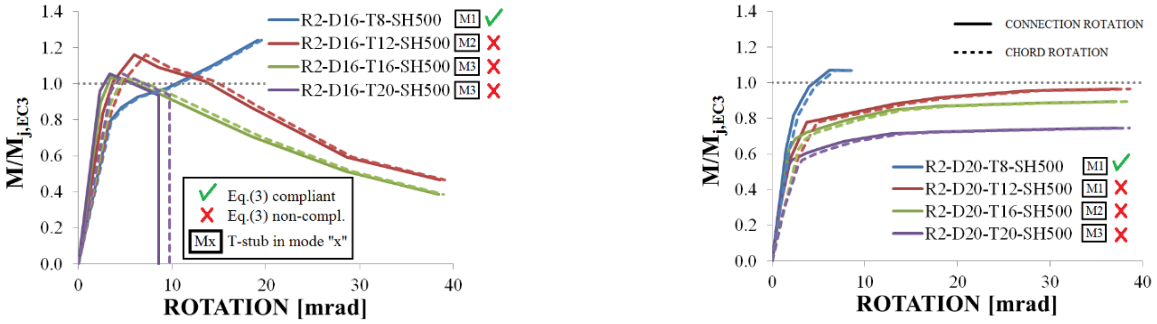

(a) M16 bolt assemblies (b) M20 bolt assemblies

Fig. 6 Effect of end-plate thickness on R2-SH500 joints: cyclic envelope curves of bending moment normalised to EC3 resistance vs connection rotation

initiation in structural components constructed from the same material. The experimental values for α and T yielded an average value at failure $\varepsilon_{p,critical}$ = 0.59 with CoV = 0.24. Chi *et al*. (2006) calculated a mean value of the parameter α equal to 2.6, corresponding to $\varepsilon_{p,critical}$ = 0.58 with a CoV = 0.17. The values obtained from these studies are consistent with values by Zangouie and Deylami (2013). Considering that the variability of critical *PEEQ* and that the cases analysed by Zangouie and Deylami (2013) are similar tothose examined in this study, the critical plastic strain equal to 0.53 was assumed as the lower bound value, given by the average *PEEQ* (i.e., 0.71) minus its standard deviation (i.e., 0.18) obtained from Zangouie and Deylami (2013). Crack initiation constitutes a limit state for FEP connections, after which a significant resisting load drop may occur. The post fracture response is highly influenced by crack propagation patterns, which depend on local material and geometrical imperfections (Wang *et al*. 2016). For these reasons, post-fracture joint behaviour is not analysed in this study and the joint response curves are truncated according to the adopted critical *PEEQ* criterion.

3.5 Moment-rotation response curves

The results obtained from FEAs are presented in terms of bending moment vs chord rotation response curves.

The connection rotation is extracted from FEA results and computed as the chord rotation θ_{chord} minus the rotation contributions of the beam θ_{beam} and of the column θ_{column} (see also Fig. 6). The rotation of the column is computed from the displacements of two points of the column at the end-plate extremities, and the beam rotation is taken as the sum of a first and second order contributions.

$$\theta_{connection} = \theta_{chord} - \theta_{column} - \theta_{beam} \tag{9}$$

$$\theta_{connection} = \arctan(\delta_{vert}/(L_{beam}/2)) - \theta_{column} - \left(arctan\left(\frac{V\left(\frac{L_{beam}}{2}\right)^2}{3EI}\right) - arctan\left(\frac{N\delta_{vert}(L_{beam}/2)^2}{2EI}\right)\right) \tag{10}$$

In order to compare joint performance, in moment-rotation response curves the bending moment is normalised to $M_{j,EC3}$, which corresponds to the bending strength calculated according to EN 1993-1-8 (CEN 2005).

4. Discussion of results

4.1 Influence of end-plate thickness

The response of FEP joint is very sensitive to the type of the dominant failure mode per bolt row. The joints with thin end-plates, i.e., characterized by T-stub mode 1, exhibit stable hysteretic loops and develop significant plastic

deformations into the end-plate. Contrarily, by increasing the thickness of the end-plate, the joint performance shifts to modes 2 and 3, where bolts fail. Fig. 4(a) shows the variation of hysteretic behaviour from mode 1 to 3 by means of an example, where T-stub failure mode 1 is analytically predicted for t = 8 mm, mode 2 for t = 12 mm and t = 16 mm, and mode 3 for t = 20 mm.

The case with t = 8 mm, which is compliant with the Eq. (3) criterion, displays energy dissipation capacity with large hysteretic loops although limited by premature fracture initiation in the fillet weld zone between the beam flange and the end-plate. This type of failure mode is observed for several analysed cases with thin end-plates and wide bolt horizontal pitch. Fig. 4(a) also shows that the cases with end-plate thickness equal to 8 mm and 12 mm provide rotation capacities limited to around 20 and 30 mrad, respectively. The joints exhibiting mode 2 and mode 3 display low energy dissipation, due to the concentration of plastic deformations in the bolts (plastic strains also occur in the welds). Owing to the gap opening of the connections, the bolts are subjected to both tensile forces and bending that are responsible of their partial bolt plasticisation (see Fig. 4(c)).

End-plate thickness is a key parameter that highly influences the behaviour of T-stub connections. Indeed, the high deformation demand is responsible for high stress concentrations in the welds between the beam flange and the end-plate (see Fig. 4(d)). The obtained results indicate that premature fracture may occur prior the achievement of chord rotation equal to 40 mrad. Instead, increasing slightly the thickness of end-plates still in the range of mode 1 but close to mode 2 can contribute to reduce the gap rotation of the connection, limiting the stress concentration and postponing the fracture initiation. It is interesting to observe that the thinner is the end-plate the larger is the developed nonlinear hardening (see Fig. 4(e)). This effect is mostly due to two phenomena: i) the large rotation around the yield lines of the bolt rows that is associated to strain hardening; ii) the membrane action developing into the end-plate when the gap rotation increases and the local deformation demand increases.

The effect of end-plate thickness on joints with 2 bolt rows and IPE 360 beam section is presented in Fig. 5 for the M16 and M20 bolt assemblies, where a vertical drop to zero of the bending moment represents the failure of bolts, while an interrupted curve indicates fracture initiation. Results for M16 assemblies (see Fig. 5(a)) show the weld fracture for the case with t = 8 mm at a rotation equal to 27 mrad. For the t = 12 mm case (i.e., bolt rows designed to exhibit mode 2), bolts sustain plastic elongation with significant pinching, namely the resistance drops to zero during load reversal. For the t = 20 mm (i.e., bolt rows designed to exhibit mode 3) premature failure of bolts occurs at 10.3 mrad. The joint designed to comply the Eq. (3) shows strain hardening up to the fracture initiation of the end-plate without plastic deformations of the bolts.

For the assemblies with M20 bolts, Fig. 5(b) shows that for the case compliant with Eq. (3) (i.e., t = 8 mm), rotation capacity is further reduced with respect to the M16 case, due to the higher rotation demand on the end-plate, with crack initiation at 17 mrad.

For the joints exhibiting either modes 2 or 3 ($t \geq 12$ mm) the energy dissipation is small, due to the bolt plasticization. The joint configurations with M24 bolts show a similar behaviour. This highlights that a significant change in FEP joint response occurs when sufficiently strong bolts are adopted.

Differently from the joints equipped with M16 bolts (see Fig. 5(a)), the joints with M20 bolts do not show any softening behaviour (see Fig. 5(b)). In particular, the joint compliant with the criterion of Eq. (3) shows premature fracture of the welds prior the completion of the loading protocol. The comparison between the simulated resistance of the joints and the strength predictions according to EN 1993-1-8 (CEN 2005) highlights that the analytical calculations accurately estimate the yield strength of joints that exhibit mode 1 per bolt row (see Fig. 6(a)). However, the simulated resistance exceeds the analytical plastic strength when the rotation increases more than 10 mrad, due to the end-plate strain hardening and the initiation of membrane effects at larger gap opening of the connection, which is not accounted for in the Components Method.

The joints showing failure mode type 3 per bolt row exhibit resistances lower than those analytically predicted. This is mostly due to the fact that the strength calculated for mode 3 accounts solely for the axial resistance of the bolts, while in the examined joints the failure of bolts is due to the combined presence of bending, shear and axial force.

The M-θ envelope curves for joints with HEA 500 beam section and M16 and M20 bolts are presented in Fig. 6. The results for M16 bolts show that only the cases with t = 12 mm and t = 16 mm sustained rotations up to 40 mrad, although associated with strength loss up to 40% of predicted resistance. For the joints equipped with M20 bolts, the cases with t = 8 mm and t = 12 mm show failure mode 1, those with t = 16 mm fail by mode 2 while the joints with t = 20 mm exhibit mode 3. For the case with t = 8 mm, the fracture initiates prior to hardening onset at $M/M_{j,EC3}$ = 1.07; for the case with t = 12 mm, the ratio $M/M_{j,EC3}$ is equal to 0.97, while the joints with t = 16 mm and t = 20 mm display $M/M_{j,EC3}$ ratios equal to 0.89 and 0.75 respectively. The large difference shown for the case with t = 20 mm (mode 3) in Fig. 6(b) is due to the fact that resistances analytically predicted for mode 2 and 3 are very similar (of course the mode 3 resistance is slightly lower). Results in Fig. 6 also show that the bending strength of the joints compliant with Eq. (3) is in line with predicted values only at small rotations, tending to increase due to end-plate strain hardening, which is limited by the fracture initiation. On the contrary, the joints not compliant with the criterion of Eq. (3) reach the $M/M_{j,EC3}$ = 1 condition at higher rotation demands.

For the joints with other beam sections, the cases with thinner end-plates (i.e., t = 8 mm and 12 mm) and M16 bolts show premature failure of the fillet welds, due to large horizontal pitch between the bolts and to significant stress concentration in the end-plate.

4.2 Influence of bolt diameter

The influence of bolt diameter is coupled with the end-plate thickness, since both variables determine the type of

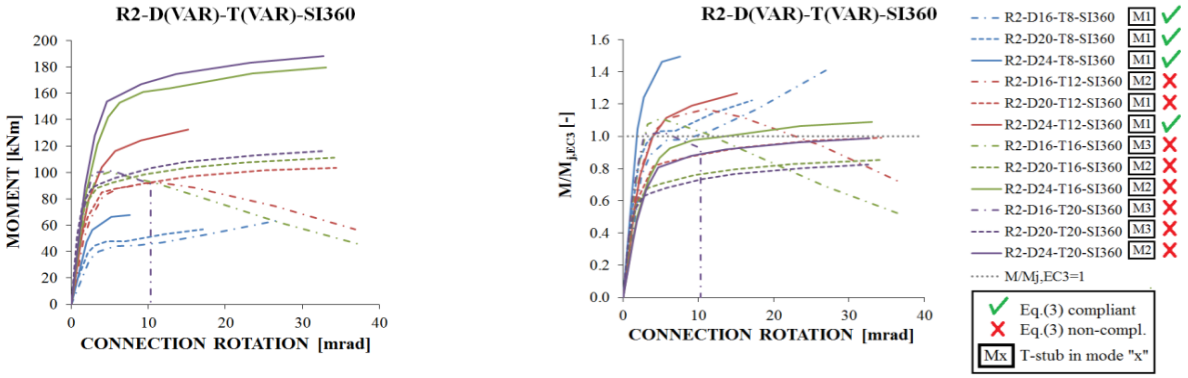

(a) Moment – connection rotation (b) Moment normalised to EC3 resistance vs. connection rotation

Fig. 7 Effect of bolt diameter on the cyclic envelope curves of R2-SI360 joints

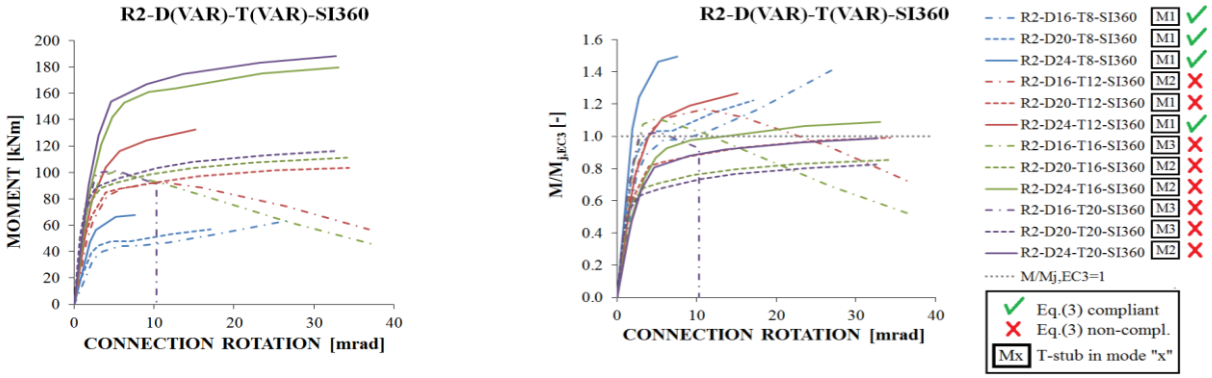

(a) Moment – connection rotation (b) Moment normalised to EC3 resistance vs. connection rotation

Fig. 8 Effect of bolt diameter on the cyclic envelope curves of R2-SH320 joints

failure mode of the equivalent T-stub per bolt row. Figs. 7 and 8 show the response curves of joints with IPE 360 and HEA 320 beams, respectively. For the cases with t = 8 mm and t = 12 mm, increasing the bolt diameter obviously leads to increasing the joint strength, although the rotation capacity decreases when transitioning from M20 to M24 bolts. It is very interesting to observe that the cases exhibiting the lower rotation capacity are characterized by failure mode type 1 (i.e., t = 8 mm). This result is only apparently contradictory, because in those cases the rotation capacity is impaired by the premature fracture of the welds, which does not occur for all cases with t > 12 mm. The bolt failure is observed only for the R2-D16-T20-SI360 case.

In terms of strength, the FEA results show that the most of the examined joints can develop $M/M_{j,EC3}$ ratios values close to or higher than 1, thus confirming the accuracy of EN 1993-1-8 (CEN 2005) predictions.

However, it is important to highlight that neither the hardening (e.g., the cases with M20 bolts) nor the softening (e.g., the cases with M16 bolts) of the response curves can be analytically predicted with the current EN1993:1-8.

The cases where the analytical predictions under-estimate the strength of the connection are those characterized by thick end-plates with failure of the bolts in the transition from mode 2 to mode 3, because of the combined actions (i.e., bending moment and tensile force) on the bolts. However, the evaluation of the damage pattern into the bolt shank requires further testing.

The joints compliant with Eq. (3) display good agreement with EC3-1-8 (CEN 2005) strength prediction (see Figs. 7 and 9), although some configurations did not withstand the full cyclic loading owing to premature fracture initiation. These findings suggest that increasing the weld strength or using full penetration welds is crucial to improve the performance under cyclic bending.

4.3 Influence of bolt rows

Numerical results indicate that increasing the number of bolt rows contributes to stabilise M-θ response, due to the positive effect of the internal force redistribution following first bolt row yielding. For instance, in the joints with M16 bolts, increasing from 2 to 4 bolt rows reduced strength softening, namely up to about 20 mrad, with large increase of the bending strength, as depicted in Fig. 9(a). Even for the cases with M24 bolts, increasing the number of bolt rows has a positive effect on both strength and rotation capacity (see Fig. 9(b)), although the overall ductility is lower than that provided by the joints with smaller bolts.

Once again, the joints compliant with the criterion given by Eq. (3) are characterized by the poorer performance, whereas non-compliant joints exhibit larger ductility even though their failure modes are mode 2 towards 3.

The results obtained from this parametric study clearly

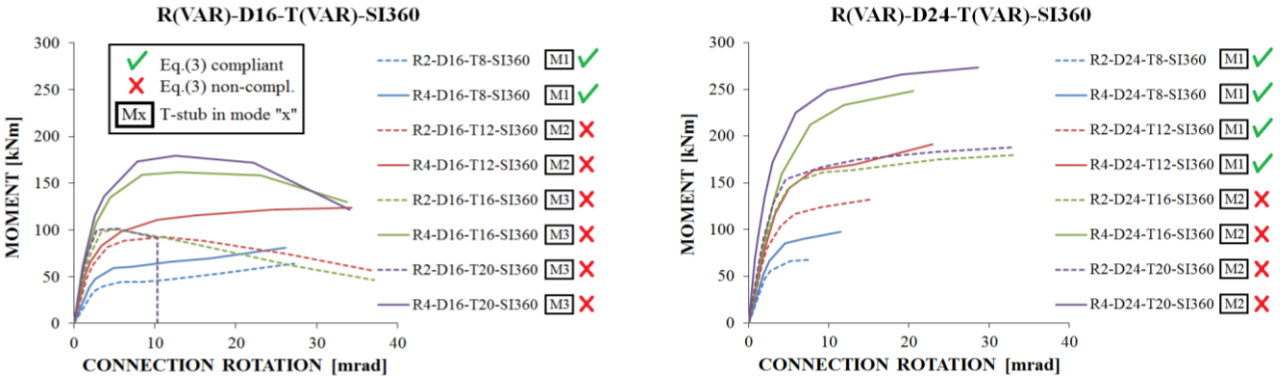

(a) M16 bolt assemblies (b) M24 bolt assemblies

Fig. 9 Effect of number of bolt rows on the cyclic envelope curves of joints with IPE 360 beam

highlight that although the criterion given by Eq. (3) (i.e., failure mode 1 per bolt row) enables the higher ductility undermonotonic bending, the most critical aspect is the detailing and the resistance of the welds. Indeed, fillet welds generally used for gravity load resisting FEP joints are inappropriate when the design criterion of Eq. (3) is used, because inducing mode 1 leads to high strain demand in the zone close to the stiffeners of the equivalent T-stub per bolt row, namely the welds. Hence, for FEP joints with conventional details, a failure mode 2 allows exploiting the larger ductility.

4.4 Performance levels

According to EN 1998-1 (CEN 2004), beam-to-column joints of the secondary structural system should have limited lateral stiffness in order to avoid any interaction with the strength and the stiffness of the primary seismic resisting system. Therefore, it is meaningful to assess in which terms the stiffness of FEP joints varies with the rotational demand and how it compares to EN 1998-1 stiffness limits. Indeed, the characterisation of stiffness degradation via the secant stiffness is useful for assessing the structural behaviour accounting for the response of joints when elastic-plastic analyses should be performed (e.g., seismic analyses). Indeed, EN1993:1-8 clause 5.1.4(5) allows simplifying the moment-rotation response curve of the joints using a bi-linear design moment-rotation relation that is obtained considering the secant stiffness. EN1993:1-8 gives also some factors (so called stiffness modification coefficients) to reduce the initial stiffness depending on the type of joints but constant for every imposed rotation. In case of FEP joints, according to EC3 the secant stiffness to be assumed in the plastic analysis is half time the initial value. Based on the experimental experience (e.g., Broderick and Thomson 2002) the secant stiffness is highly dependent on the rotation and the simplification of EC3 can be largely inaccurate. To this end, the degradation of joint stiffness is quantified for different values of the chord rotation θ (i.e., for 0%, 1%, 2%, 3% and 4%) by means of the ratio between joint secant stiffness ($S_{sec,\theta}$) at each θ and the initial stiffness ($S_{j,ini,EC3}$) calculated according to EN 1993-1-8 (CEN 2005). With this regard, it should be noted that the value $S_{sec,\theta=0\%}$calculated at θ = 0% corresponds to the initial stiffness. Thus, the ratio $S_{sec,\theta=0\%}/S_{j,ini,EC3}$ allows identifying the cases where the EC3 analytical prediction mismatch the stiffness of the connection. Indeed, as shown by Da Silva *et al*. (2004) and Girão Coelho and Bijlaard (2007), the initial stiffness prediction obtained according to EN 1993-1-8 can be inaccurate.

As reported in Tables 3 and 4, performance levels STF1 through STF5 are proposed and defined *ad hoc* based on intervals of the ratios $S_{sec,\theta}/S_{j,ini,EC3}$.Theperformance level STF1 (being STF the acronym used for stiffness) is adopted to identify the joints with secant stiffness $S_{sec,\theta}$ at chord rotation θ higher than the initial stiffness $S_{j,ini,EC3}$ predicted by EN 1993-1-8. STF2 identifies the cases with secant stiffness within the range 0.80-1.00 times $S_{j,ini,EC3}$. STF3 identifies the cases with secant stiffness within the range 0.50-0.80 times $S_{j,ini,EC3}$. STF4 corresponds to joints with secant stiffness within the range 0.20-0.50 times $S_{j,ini,EC3}$ and level STF5 is indicative of a joint secant stiffness at chord rotation θ that is below 20% of the EN 1993-1-8 initial joint stiffness predicted value. As shown in the Tables 3 and 4, the STF1 level corresponds to low rotation demands, while STF5 level is associated to the higher values of chord rotation.

The comparison in terms of initial stiffness between the numerical results and the EN1993-1-8 predictions confirms noticeable differences, as recognized by different studies (e.g., Broderick and Thomson 2002, Aribert *et al*. 2004, Da Silva *et al*. 2004, Girão Coelho and Bijlaard 2007). The results in terms of $S_{sec,\theta}/S_{j,ini,EC3}$ ratios at θ = 0 for the cases with 2 bolt rows indicate an average value of 1.15 and a standard deviation of 0.41, whereas an average value of 1.20 and a standard deviation of 0.44 for the cases with 4 bolt rows. Despite this large variability, the values obtained in this study fall within the expected range as reported by other Authors.

The numerical results for joints with 2 bolt rows reported in Table 3 show that stiffness degradation is more severe for the configurations with the smaller bolt diameter and the thicker end-plates, typically leading to performance level STF5 at θ = 3% (i.e., $S_{sec,}\theta/S_{j,ini,EC3}$ < 0.2). The stiffness of the joints with M16 bolts is lower than 20% of the initial EC3 stiffness at θ = 4%. The joints with M20 bolts and the larger beam sections (both IPE and HEA) are characterized by performance level STF4 at θ = 4% (i.e.,

Table 3 Stiffness ratios, classification and performance levels of joints with 2 bolt rows

R	D	T	S	Stiffness Ratio					Stiffness Classification				
				$S_{sec,\theta}/S_{j,ini,EC3}$					$S_{sec,\theta}/S_{j,pin,EC3}$				
[-]	[mm]	[mm]	[-]	θ=0%	θ=1%	θ=2%	θ=3%	θ=4%	θ=0%	θ=1%	θ=2%	θ=3%	θ=4%
2	16	8	I220	0.96	0.72	0.42	0.31	0.00	7.19	5.37	3.14	2.31	0.00
			I360	0.85	0.40	0.24	0.19	0.00	4.54	2.13	1.27	1.03	0.00
			H320	1.73	1.00	0.57	0.44	0.38	2.38	1.38	0.78	0.60	0.52
			H500	1.10	0.49	0.31	0.00	0.00	1.34	0.60	0.38	0.00	0.00
		12	I220	0.76	0.65	0.47	0.33	0.00	9.33	8.02	5.73	4.02	0.00
			I360	0.79	0.52	0.26	0.14	0.08	6.48	4.27	2.14	1.19	0.68
			H320	1.32	0.96	0.48	0.28	0.16	3.65	2.65	1.32	0.76	0.45
			H500	1.01	0.47	0.19	0.09	0.05	2.43	1.14	0.46	0.21	0.12
		16	I220	0.70	0.62	0.50	0.36	0.24	10.21	9.05	7.32	5.25	3.55
			I360	0.80	0.57	0.21	0.11	0.06	7.43	5.28	1.97	0.99	0.56
			H320	1.22	0.81	0.35	0.19	0.11	4.41	2.93	1.27	0.68	0.42
			H500	1.00	0.38	0.14	0.07	0.04	3.01	1.14	0.42	0.21	0.12
		20	I220	0.71	0.63	0.54	0.36	0.22	10.92	9.81	8.29	5.59	3.37
			I360	0.82	0.52	0.00	0.00	0.00	7.90	5.08	0.00	0.00	0.00
			H320	1.21	0.74	0.31	0.17	0.10	4.85	2.95	1.23	0.68	0.41
			H500	0.98	0.34	0.00	0.00	0.00	3.22	1.13	0.00	0.00	0.00
	20	8	I220	1.04	0.82	0.48	0.00	0.00	7.98	6.28	3.69	0.00	0.00
			I360	1.02	0.45	0.24	0.00	0.00	5.73	2.52	1.38	0.00	0.00
			H320	2.00	1.10	0.60	0.47	0.40	2.81	1.55	0.85	0.66	0.57
			H500	1.63	0.58	0.00	0.00	0.00	1.92	0.69	0.00	0.00	0.00
		12	I220	0.76	0.69	0.50	0.37	0.00	9.82	8.93	6.47	4.75	0.00
			I360	0.83	0.52	0.27	0.19	0.14	7.25	4.52	2.36	1.64	1.27
			H320	1.45	0.95	0.51	0.36	0.28	4.20	2.76	1.49	1.06	0.82
			H500	1.24	0.49	0.25	0.18	0.13	3.14	1.23	0.64	0.44	0.34
		16	I220	0.69	0.64	0.50	0.39	0.29	10.70	9.96	7.76	6.12	4.52
			I360	0.81	0.49	0.25	0.19	0.14	8.11	4.88	2.55	1.88	1.35
			H320	1.29	0.73	0.43	0.30	0.23	4.98	2.84	1.65	1.17	0.89
			H500	1.03	0.39	0.21	0.14	0.11	3.34	1.25	0.68	0.46	0.35
		20	I220	0.67	0.57	0.48	0.37	0.28	11.17	9.56	8.04	6.20	4.74
			I360	0.82	0.45	0.25	0.18	0.14	8.59	4.75	2.66	1.87	1.47
			H320	1.21	0.69	0.41	0.28	0.22	5.22	2.96	1.78	1.19	0.94
			H500	1.17	0.38	0.20	0.13	0.10	4.19	1.36	0.72	0.47	0.36
	24	8	I220	1.17	1.02	0.62	0.00	0.00	9.03	7.88	4.77	0.00	0.00
			I360	1.12	0.57	0.00	0.00	0.00	6.36	3.25	0.00	0.00	0.00
			H320	2.44	1.37	0.76	0.00	0.00	3.47	1.94	1.08	0.00	0.00
			H500	1.53	0.00	0.00	0.00	0.00	1.92	0.00	0.00	0.00	0.00
		12	I220	0.78	0.76	0.61	0.43	0.00	10.38	10.07	8.06	5.68	0.00
			I360	0.88	0.63	0.35	0.00	0.00	7.96	5.72	3.18	0.00	0.00
			H320	1.61	1.15	0.66	0.47	0.37	4.77	3.41	1.96	1.40	1.09
			H500	1.20	0.61	0.00	0.00	0.00	3.13	1.59	0.00	0.00	0.00
		16	I220	0.69	0.68	0.59	0.45	0.00	11.02	10.89	9.43	7.29	0.00
			I360	0.82	0.67	0.40	0.27	0.21	8.60	7.04	4.25	2.80	2.16
			H320	1.38	1.12	0.66	0.46	0.36	5.52	4.50	2.64	1.84	1.44
			H500	1.10	0.60	0.34	0.23	0.18	3.72	2.04	1.13	0.77	0.59
		20	I220	0.66	0.65	0.58	0.46	0.36	11.39	11.32	10.07	8.04	6.33
			I360	0.81	0.67	0.38	0.26	0.20	9.04	7.44	4.23	2.93	2.26
			H320	1.33	1.04	0.61	0.43	0.34	5.97	4.70	2.74	1.94	1.52
			H500	1.07	0.56	0.31	0.23	0.17	4.05	2.11	1.18	0.86	0.63

Table 4 Stiffness ratios, classification and performance levels of joints with 4 bolt rows

R	D	T	S	Stiffness Ratio					Stiffness Classification				
				$S_{sec,\theta}/S_{j,ini,EC3}$					$S_{sec,\theta}/S_{j,pin,EC3}$				
[-]	[mm]	[mm]	[-]	θ=0%	θ=1%	θ=2%	θ=3%	θ=4%	θ=0%	θ=1%	θ=2%	θ=3%	θ=4%
4*	16	8	I220	1.04	0.82	0.48	0.35	0.00	7.33	5.81	3.36	2.47	0.00
			I360	1.03	0.58	0.33	0.25	0.00	5.29	2.96	1.67	1.30	0.00
			H320	2.01	1.18	0.68	0.53	0.44	2.49	1.47	0.84	0.65	0.54
			H500	1.37	0.66	0.39	0.00	0.00	1.56	0.76	0.45	0.00	0.00
		12	I220	0.78	0.69	0.53	0.37	0.27	9.33	8.28	6.38	4.39	3.27
			I360	0.88	0.60	0.35	0.24	0.19	7.03	4.78	2.79	1.95	1.48
			H320	1.47	1.10	0.61	0.44	0.32	3.77	2.82	1.57	1.11	0.82
			H500	1.17	0.68	0.35	0.22	0.15	2.72	1.58	0.81	0.51	0.35
		16	I220	0.71	0.65	0.55	0.41	0.30	10.28	9.35	7.86	5.86	4.39
			I360	0.85	0.70	0.43	0.28	0.17	7.80	6.47	3.94	2.53	1.56
			H320	1.34	1.09	0.66	0.46	0.32	4.57	3.71	2.25	1.55	1.08
			H500	1.14	0.72	0.33	0.19	0.08	3.35	2.11	0.98	0.57	0.24
		20	I220	0.70	0.64	0.56	0.42	0.31	10.79	9.89	8.68	6.48	4.84
			I360	0.85	0.73	0.44	0.29	0.15	8.23	7.03	4.30	2.78	1.47
			H320	1.31	1.03	0.68	0.46	0.28	5.04	4.00	2.64	1.77	1.08
			H500	1.13	0.68	0.30	0.16	0.07	3.66	2.21	0.97	0.52	0.23
	20	8	I220	1.10	0.96	0.54	0.00	0.00	7.94	6.91	3.91	0.00	0.00
			I360	1.14	0.63	0.35	0.00	0.00	5.97	3.29	1.85	0.00	0.00
			H320	2.24	1.31	0.75	0.60	0.00	2.81	1.65	0.95	0.75	0.00
			H500	1.48	0.73	0.00	0.00	0.00	1.71	0.84	0.00	0.00	0.00
		12	I220	0.77	0.74	0.57	0.41	0.00	9.62	9.22	7.06	5.06	0.00
			I360	0.90	0.68	0.40	0.00	0.00	7.47	5.69	3.30	0.00	0.00
			H320	1.70	1.23	0.71	0.49	0.38	4.36	3.14	1.83	1.27	0.97
			H500	1.28	0.71	0.38	0.27	0.20	3.07	1.70	0.91	0.65	0.49
		16	I220	0.70	0.67	0.56	0.44	0.34	10.62	10.15	8.50	6.67	5.11
			I360	0.86	0.68	0.44	0.31	0.24	8.27	6.56	4.19	3.00	2.30
			H320	1.45	1.06	0.73	0.51	0.37	5.13	3.76	2.59	1.80	1.32
			H500	1.14	0.69	0.39	0.27	0.21	3.51	2.11	1.19	0.84	0.64
		20	I220	0.68	0.65	0.56	0.43	0.34	11.10	10.57	9.20	7.02	5.50
			I360	0.85	0.68	0.44	0.31	0.24	8.66	6.98	4.53	3.20	2.45
			H320	1.34	1.02	0.69	0.51	0.39	5.44	4.13	2.79	2.07	1.58
			H500	1.27	0.64	0.38	0.26	0.20	4.37	2.20	1.32	0.90	0.69
	24	8	I220	1.25	1.17	0.73	0.00	0.00	9.12	8.59	5.37	0.00	0.00
			I360	1.31	0.82	0.00	0.00	0.00	6.94	4.33	0.00	0.00	0.00
			H320	2.88	1.69	0.94	0.00	0.00	3.62	2.13	1.18	0.00	0.00
			H500	1.90	0.00	0.00	0.00	0.00	2.22	0.00	0.00	0.00	0.00
		12	I220	0.82	0.80	0.65	0.48	0.00	10.37	10.21	8.30	6.14	0.00
			I360	0.97	0.82	0.50	0.36	0.00	8.23	6.94	4.24	3.07	0.00
			H320	1.84	1.39	0.81	0.59	0.47	4.93	3.73	2.15	1.59	1.25
			H500	1.42	0.85	0.45	0.00	0.00	3.47	2.08	1.10	0.00	0.00
		16	I220	0.71	0.71	0.63	0.48	0.00	10.95	10.95	9.82	7.51	0.00
			I360	0.89	0.81	0.57	0.41	0.00	8.78	8.00	5.59	4.05	0.00
			H320	1.56	1.29	0.86	0.62	0.47	5.65	4.68	3.13	2.25	1.71
			H500	1.28	0.87	0.51	0.35	0.26	4.04	2.75	1.60	1.09	0.83
		20	I220	0.67	0.67	0.61	0.49	0.40	11.35	11.34	10.28	8.23	6.68
			I360	0.87	0.79	0.57	0.40	0.31	9.10	8.33	5.98	4.26	3.28
			H320	1.46	1.24	0.90	0.66	0.50	6.07	5.14	3.73	2.73	2.09
			H500	1.24	0.86	0.52	0.37	0.28	4.37	3.05	1.85	1.30	1.00

Strength performance		Strength classification	
Level	$S_{sec,\theta}/S_{j,ini,EC3}$	Classification	$S_{sec,\theta}/S_{j,pin,EC3}$
STF1	> 1.00	Semi rigid	> 1.00
STF2	0.80-1.00	Nominally pinned	0.00-1.00
STF3	0.50-0.80	Failure	0.00
STF4	0.20-0.50		
STF5	0.00-0.20		

Strength performance		Strength classification	
Level	$S_{sec,\theta}/S_{j,ini,EC3}$	Classification	$S_{sec,\theta}/S_{j,pin,EC3}$
STF1	> 1.00	Semi rigid	> 1.00
STF2	0.80-1.00	Nominally pinned	0.00-1.00
STF3	0.50-0.80	Failure	0.00
STF4	0.20-0.50		
STF5	0.00-0.20		

* 3 bolt rows in the case of IPE 220 profiles

$0.2 < S_{sec,\theta}/S_{j,ini,EC3} < 0.5$). The joints with M24 bolts provide performance level STF4 at θ = 3% and θ = 4%, thus retaining the higher secant stiffness under cyclic actions.

In order to investigate for which levels of rotation the stiffness of the damaged joints is negligible, $S_{sec,\theta}$ is also compared to stiffness limit for nominally pinned joints $S_{j,pin,EC3}$ as classified by EN 1993-1-8 (CEN 2005), where $S_{j,pin,EC3} = 0.5EI_b/L_b$ (being E the elastic modulus of the steel, I_b the second moment of area of the beam and L_b the beam length). Indeed, if the secant stiffness of the joints is larger than $S_{j,pin,EC3}$, the damaged joints have still enough stiffness (i.e., they can still behave as semi-rigid) that should be accounted for in the structural analysis. If the $S_{sec,\theta}/S_{j,pin,EC3}$ ratios are smaller than 1, the degraded stiffness is negligible, and it can be disregarded in the structural analysis. The connection is obviously failed if the ratios are equal to zero.

The results in Table 3 show that the joints with the smaller bolt diameters undergo significant stiffness degradation. The higher values at θ close to 0% are due to the bolt preloading, which significantly increases joint initial stiffness with respect to the EN 1993-1-8 prediction. The results show that FEP joints behave as semi-rigid at

Table 5 Strength ratios, classification and performance levels of joints with 2 bolt rows

R	D	T	S	Strength Ratio				Strength Classification			
[-]	[mm]	[mm]	[-]	$M_{\theta,chord}/M_{j,Rm,EC3}$ [-]				$M_{\theta,chord}/M_{j,pin,EC3}$ [-]			
				θ=1%	θ=2%	θ=3%	θ=4%	θ=1%	θ=2%	θ=3%	θ=4%
2	16	8	I220	0.84	0.98	1.08	0.00	0.72	0.84	0.93	0.00
			I360	0.98	1.17	1.41	0.00	0.47	0.56	0.68	0.00
			H320	1.01	1.15	1.33	1.51	0.27	0.30	0.35	0.40
			H500	0.97	1.24	0.00	0.00	0.18	0.23	0.00	0.00
		12	I220	0.69	0.99	1.06	0.00	1.06	1.53	1.62	0.00
			I360	1.11	1.12	0.94	0.72	0.94	0.94	0.79	0.60
			H320	1.23	1.24	1.05	0.82	0.51	0.51	0.44	0.34
			H500	1.09	0.87	0.59	0.47	0.35	0.28	0.19	0.15
		16	I220	0.67	1.09	1.17	1.04	1.21	1.97	2.12	1.89
			I360	1.11	0.91	0.69	0.51	1.06	0.87	0.66	0.49
			H320	1.05	0.90	0.74	0.60	0.57	0.49	0.40	0.32
			H500	0.95	0.70	0.51	0.39	0.35	0.26	0.19	0.14
		20	I220	0.60	1.02	1.04	0.83	1.31	2.23	2.26	1.81
			I360	1.02	0.00	0.00	0.00	1.07	0.00	0.00	0.00
			H320	1.05	0.88	0.73	0.59	0.57	0.48	0.40	0.32
			H500	0.94	0.00	0.00	0.00	0.34	0.00	0.00	0.00
	20	8	I220	0.96	1.12	0.00	0.00	0.83	0.96	0.00	0.00
			I360	1.03	1.22	0.00	0.00	0.51	0.60	0.00	0.00
			H320	1.08	1.24	1.45	1.66	0.28	0.33	0.38	0.44
			H500	1.07	0.00	0.00	0.00	0.19	0.00	0.00	0.00
		12	I220	0.60	0.91	0.99	0.00	1.14	1.72	1.89	0.00
			I360	0.84	0.93	0.97	0.99	0.93	1.03	1.08	1.10
			H320	0.83	0.96	1.03	1.06	0.49	0.57	0.61	0.63
			H500	0.83	0.92	0.96	0.97	0.35	0.39	0.40	0.41
		16	I220	0.53	0.86	0.93	0.99	1.26	2.05	2.22	2.37
			I360	0.71	0.80	0.83	0.85	0.98	1.10	1.14	1.18
			H320	0.78	0.92	0.97	0.99	0.54	0.64	0.67	0.69
			H500	0.79	0.87	0.88	0.90	0.38	0.41	0.42	0.43
		20	I220	0.65	0.77	0.86	0.91	1.81	2.15	2.39	2.52
			I360	0.68	0.77	0.80	0.82	1.02	1.15	1.20	1.23
			H320	0.67	0.78	0.81	0.83	0.57	0.66	0.69	0.70
			H500	0.67	0.72	0.74	0.75	0.39	0.42	0.42	0.43
	24	8	I220	1.24	1.52	0.00	0.00	1.05	1.28	0.00	0.00
			I360	1.49	0.00	0.00	0.00	0.72	0.00	0.00	0.00
			H320	1.43	1.61	0.00	0.00	0.38	0.42	0.00	0.00
			H500	0.00	0.00	0.00	0.00	0.00	0.00	0.00	0.00
		12	I220	0.71	1.06	1.21	0.00	1.34	2.02	2.29	0.00
			I360	1.19	1.27	0.00	0.00	1.32	1.41	0.00	0.00
			H320	1.12	1.28	1.38	1.43	0.66	0.76	0.82	0.85
			H500	1.15	0.00	0.00	0.00	0.48	0.00	0.00	0.00
		16	I220	0.53	0.92	1.08	0.00	1.46	2.52	2.95	0.00
			I360	0.86	0.99	1.06	1.09	1.51	1.74	1.86	1.91
			H320	0.84	1.02	1.10	1.13	0.81	0.99	1.06	1.09
			H500	0.94	1.02	1.07	1.09	0.62	0.68	0.71	0.72
		20	I220	0.47	0.87	1.04	1.09	1.48	2.72	3.25	3.41
			I360	0.81	0.92	0.96	0.99	1.63	1.85	1.95	2.00
			H320	0.83	1.02	1.10	1.13	0.86	1.05	1.13	1.17
			H500	0.91	1.00	1.05	1.08	0.64	0.71	0.74	0.76

Strength performance		Strength classification	
Level	$M_{\theta,chord}/M_{j,Rm,EC3}$	Classification	$M_{\theta,chord}/M_{j,pin,EC3}$
STR1	> 1.00	Partial Strength	> 1.00
STR2	0.80-1.00	Nominally Pinned	0.00-1.00
STR3	0.50-0.80	Failure	0.00
STR4	0.20-0.50		
STR5	0.00-0.20		

Table 6 Strength ratios, classification and performance levels of joints with 4 bolt rows

R	D	T	S	Strength Ratio				Strength Classification			
[-]	[mm]	[mm]	[-]	$M_{\theta,chord}/M_{j,Rm,EC3}$ [-]				$M_{\theta,chord}/M_{j,pin,EC3}$ [-]			
				θ=1%	θ=2%	θ=3%	θ=4%	θ=1%	θ=2%	θ=3%	θ=4%
4*	16	8	I220	0.58	0.68	0.73	0.00	0.78	0.91	0.98	0.00
			I360	1.21	1.39	1.62	0.00	0.64	0.74	0.86	0.00
			H320	0.54	0.61	0.72	0.80	0.29	0.32	0.38	0.42
			H500	1.21	1.42	0.00	0.00	0.23	0.27	0.00	0.00
		12	I220	0.67	0.97	1.08	1.06	1.10	1.60	1.78	1.74
			I360	0.90	1.07	1.12	1.14	1.04	1.23	1.29	1.31
			H320	1.08	1.20	1.28	1.26	0.55	0.61	0.65	0.64
			H500	1.16	1.16	1.14	1.04	0.47	0.47	0.46	0.42
		16	I220	0.60	1.01	1.13	1.10	1.26	2.12	2.37	2.31
			I360	0.96	1.16	1.13	0.93	1.43	1.72	1.68	1.38
			H320	0.95	1.21	1.25	1.16	0.69	0.88	0.91	0.84
			H500	1.05	1.04	0.89	0.52	0.61	0.60	0.51	0.30
		20	I220	0.52	0.91	1.02	1.01	1.33	2.33	2.62	2.60
			I360	0.84	1.10	1.06	0.75	1.44	1.90	1.82	1.29
			H320	0.94	1.24	1.25	1.01	0.78	1.03	1.04	0.84
			H500	1.08	0.94	0.75	0.45	0.67	0.58	0.47	0.28
	20	8	I220	0.65	0.78	0.00	0.00	0.87	1.04	0.00	0.00
			I360	1.37	1.53	0.00	0.00	0.73	0.81	0.00	0.00
			H320	0.60	0.68	0.82	0.00	0.32	0.36	0.43	0.00
			H500	1.33	0.00	0.00	0.00	0.25	0.00	0.00	0.00
		12	I220	0.48	0.75	0.82	0.00	1.20	1.86	2.03	0.00
			I360	1.02	1.19	0.00	0.00	1.25	1.44	0.00	0.00
			H320	0.99	1.18	1.25	1.27	0.58	0.69	0.73	0.75
			H500	1.15	1.26	1.32	1.35	0.50	0.55	0.58	0.59
		16	I220	0.50	0.89	1.02	1.06	1.27	2.27	2.60	2.69
			I360	0.73	0.93	1.00	1.02	1.45	1.85	1.98	2.04
			H320	0.87	1.12	1.25	1.23	0.72	0.92	1.03	1.01
			H500	0.88	1.05	1.10	1.13	0.61	0.73	0.77	0.78
		20	I220	0.49	0.83	0.99	1.03	1.41	2.39	2.83	2.96
			I360	0.65	0.86	0.91	0.93	1.51	1.99	2.12	2.17
			H320	0.71	0.96	1.05	1.09	0.80	1.08	1.19	1.23
			H500	0.75	0.87	0.92	0.94	0.67	0.78	0.82	0.84
	24	8	I220	0.79	1.06	0.00	0.00	1.06	1.42	0.00	0.00
			I360	1.81	0.00	0.00	0.00	0.96	0.00	0.00	0.00
			H320	0.78	0.86	0.00	0.00	0.41	0.46	0.00	0.00
			H500	0.00	0.00	0.00	0.00	0.00	0.00	0.00	0.00
		12	I220	0.56	0.90	1.00	0.00	1.38	2.23	2.48	0.00
			I360	1.26	1.48	1.67	0.00	1.53	1.80	2.03	0.00
			H320	0.71	0.83	0.89	0.96	0.72	0.83	0.90	0.97
			H500	1.40	1.53	0.00	0.00	0.61	0.67	0.00	0.00
		16	I220	0.54	0.96	1.12	0.00	1.44	2.58	3.02	0.00
			I360	0.81	1.18	1.26	0.00	1.70	2.47	2.63	0.00
			H320	0.71	0.96	1.03	1.05	0.91	1.22	1.32	1.34
			H500	1.07	1.21	1.28	1.30	0.84	0.95	1.00	1.02
		20	I220	0.39	0.78	0.93	0.98	1.40	2.76	3.32	3.48
			I360	0.68	0.99	1.05	1.08	1.83	2.64	2.82	2.90
			H320	0.78	1.13	1.24	1.27	1.00	1.45	1.59	1.63
			H500	0.83	1.01	1.08	1.10	0.92	1.12	1.19	1.21

Strength performance		Strength classification	
Level	$M_{\theta,chord}/M_{j,Rm,EC3}$	Classification	$M_{\theta,chord}/M_{j,pin,EC3}$
STR1	> 1.00	Partial Strength	> 1.00
STR2	0.80-1.00	Nominally Pinned	0.00-1.00
STR3	0.50-0.80	Failure	0.00
STR4	0.20-0.50		
STR5	0.00-0.20		

* 3 bolt rows in the case of IPE 220 profiles

low rotational demand, (i.e., the initial stiffness is higher than the upper bound value for pinned joints). However, as the imposed chord rotation θ increases, the stiffness degrades (i.e., $S_{sec,\theta}/S_{j,pin,EC3}$ ratios become lower than 1). This is more noticeable for joints with M16 bolts, which display the higher stiffness degradation, than for M20 and M24 cases, which tend to behave as semi-rigid joints for larger chord rotations. Of course, the joints with the shallower beams are more prone to be semi-rigid, as well as those with larger number of bolt rows (e.g., R4 joints). The results obtained for R4 joints (i.e., the joints with 4 bolt rows except for IPE220 where only 3 rows are technologically feasible) are reported in Table 4, where it

can be recognized that adding inner bolt rows reduces the stiffness degradation. Indeed, at θ = 4% the majority of non-failed joints exhibit performance level STF4 (i.e., 0.2 < $S_{sec,\theta}/S_{j,ini,EC3} \leq 0.5$).

The evolution of joint strength under cyclic action was quantified by means of the ratios $M_{\theta,chord}/M_{j,Rm,EC3}$, where $M_{\theta,chord}$ is the resistance at chord rotation θ and $M_{j,Rm,EC3}$ is the average strength calculated according to EN 1993-1-8 (CEN 2005). Similarly to what has been assumed for the stiffness, a set of performance levels was proposed for the strength ratios. As reported in Tables 5 and 6, the performance level STR1 (being STR the acronym used for strength) is adopted to identify the joints with bending strength $M_{\theta,chord}$ at chord rotation θ is higher than the EN 1993-1-8 bending strength prediction $M_{j,Rm,EC3}$. STR2 identifies the cases with moment resistance within the range 0.80-1.00 times $M_{j,Rm,EC3}$. STR3 identifies the cases with $M_{\theta,chord}$ within the range 0.50-0.80 times $M_{j,Rm,EC3}$. STR4 corresponds to joints with bending strength within the range 0.20-0.50 times $M_{j,Rm,EC3}$ and STR5 is attributed when the bending strength at chord rotation θ is lower than 20% of the EN 1993-1-8 bending strength.

STR1 performance level is associated to low rotation demand, while level STR5 corresponds to the higher chord rotational demand values (see Tables 5 and 6 for more details).

Similarly to what has been shown for the secant stiffness, the bending strength $M_{\theta,chord}$ is also compared to the upper bound limit resistance for pinned joints $M_{j,pin,EC3}$ calculated according to EN 1993-1-8 (CEN 2005), in order to examine the levels of rotation leading to negligible resistance. Indeed, if $M_{\theta,chord}$ is larger than $M_{\mathrm{j,pin,EC3}}$, the damaged joints can be considered as partial strength and its bending resistance can be accounted for in the structural analysis. If the $M_{\theta,chord}/M_{j,pin,EC3}$ ratios are smaller than 1, the resistance of the damaged joint is negligible, and it can be disregarded in the structural analysis, while the joint is failed if the ratios are equal to zero.

The results summarized in Table 5 show significant strength degradation for the joints with smaller bolt diameters and thicker end-plates. Indeed, for joints with M16 bolts and $t \geq 16$ mm, the strength degradation at θ = 4% is considerable due to damage of bolts. Fracture initiation was observed for the cases with thinner plates (i.e., t = 8 mm) due to higher rotational demand on the plates. The best performance is provided by the joints with M20 bolts, which display performance levels STR1 and STR2. The joints with compact beam sections and larger bolt diameters (e.g., M24) exhibit partial-strength behaviour. The joints with t = 8 mm generally behave as nominally pinned ($M_{\theta,chord}/M_{j,pin,EC3} < 1$) even at low rotation demands, whereas for $t \geq 12$ mm and IPE profiles for the beam behave as partial-strength, while those equipped with HE profiles ranging between HEA 320 and HEA 500 behave as pinned joints (i.e., $M_{\theta,chord}/M_{j,pin,EC3} < 1$). For 4 bolt row configurations, strength ratios at 3% and 4% rotational demand are higher than those of the corresponding 2 bolt row joints, see Table 6. In particular, the results indicate that increasing the number of bolt rows improves the joint performance when small bolt diameter are used. For joint with M20 or M24 bolts, at θ = 4%, strength ratios are generally greater than 1.

4.5 Consequences for design

The response of FEP joints under cyclic actions showed that the most of analysed joint configurations can sustain cyclic actions compatible with those induced by seismic events leading to chord rotations up to 4%, while maintaining strength levels consistent with EN 1993-1-8 (CEN 2005) prediction. However, some joints designed to enforce failure mode 1 at each bolt row, namely those with the thinner end-plates (t = 8 mm) experience premature fracture in the welds between the beam flange and the end-plate, which occur prior to θ =4%.

Hence, the revised EC3-1-8 criterion expressed in Eq. (3) for selecting end-plate thicknesses inducing mode 1, accounting for material variability and strain hardening is not sufficient for FEP joints in seismic zones. Indeed, the criterion given by Eq. (3) was formerly developed for primary resisting joints and detailed with full penetration welds (D'Aniello *et al*. 2017a).

Considering that both joints and connected members of the secondary structural system are subjected to the same interstorey drift demand of the primary structure, the failure of the secondary joints under seismic action is not acceptable. Therefore, in order to guarantee adequate ductility, it is necessary to impose specific requirements on the welds, which should be able to accommodate large strain demand without collapse. This type of performance can be obtained if the weld zone is designed with adequate overstrength in relation to the ultimate resistance of the connected elements. Considering the dimension of the beams typically used for building frames, full penetration welds between the beam flange and the end-plate would be more effective than the commonly adopted fillet welds. Alternatively, if fillet welds should be technologically adopted, the minimum required strength for the fillet welds should be determined as follows

$$R_{d,weld} = \gamma_{sh} \cdot \gamma_{ov} \cdot R_{y,d} \quad (11)$$

where $R_{d,weld}$ is the resistance of the weld, $R_{y,d}$ is the maximum between the resistance of the beam flange and that of the end-plate and γ_{sh} and γ_{ov} are the corresponding strain hardening and overstrength factors, which can be respectively assumed equal to 1.1 and 1.25 as provided by EN 1998-1.

The analysis of the obtained results also indicates that the joints showing failure mode 2 but close to mode 1 are generally capable of withstanding the applied cyclic loading up to 40 mrad, which is due to a lower stress concentration in the welds, thanks to the smaller rotation between the beam flange and end-plate. However, designing FEP joints in mode 2 close to mode 1 may lead to loss of strength at higher rotation demands (see Fig. 6(a)) owing to the damage of bolts.

Designing FEP joints in seismic zones for achieving high ductility in T-stub mode 1 appears to constitute the best design strategy, as long as the welds are designed with appropriate overstrength. This allows the bolt components to remain elastic, while the ductility is mainly provided by

the end-plate, hence avoiding softening due to the bolt deterioration. The adoption of thin end-plates inducing mode 1 also leads to joints with low bending strength, which is more in line with nominally pinned behaviour and with the typical design assumption of disregarding FEP joint stiffness and strength for the global behaviour of the structure. In the light of the obtained results, to achieve rotational capacities up to 40 mrad the thickness of end-plate should be selected with within the range 1/2 - 2/3 the bolt diameter, which guarantee T-Stub mode 1, provided that full penetration welds are used. For what concerns the bolts, the use of bigger diameters (e.g., M20 and M24) and spaced in order to minimize the group effect per row is preferable to allow accommodating large connection opening. Finally, to enhance both strength and rotation capacity is more convenient to use 4 bolt rows instead of 2.

FEA results indicate that at high rotational demand, the flexural behaviour of the joints is generally more consistent with the assumption of disregarding its contribution, whereas at lower demand, the high secant stiffness leads to semi-rigid joint behaviour. Joints with small bolt diameters (i.e., M16) behave as nominally pinned at θ = 3% and θ = 4%, while remaining semi-rigid for smaller demands. FEP joints with medium/large bolt diameters tend to behave as semi-rigid joints even at θ = 4%. Considering that during a seismic event, joints may be subjected to both low and high rotation demands, explicit modelling of FEP beam-column joints is recommendable for accurate structural analysis.

5. Conclusions

In this paper, the results of parametric finite element analyses on gravity load designed FEP beam-column joints under cyclic bending are described and discussed, with the aim to evaluate the suitability of this type of joint in seismic areas. A design criterion formerly developed for partial strength dissipative joints and based on the EN 1993-1-8 (CEN 2005) is numerically investigated. The effects of geometrical and mechanical parameters are analysed and the evolution of both strength and stiffness in cyclic bending is quantified by means of ad-hoc defined performance levels. The obtained results are compared to EN 1993-1-8 (CEN 2005) limits for nominally pinned joints, to evaluate the joint compliance with Eurocode classification criteria. In light of the obtained results, the following remarks can be drawn:

- The response of FEP joints under cyclic actions is influenced by the joint details and the failure mode of the equivalent T-stub per bolt row;
- Adopting thin end-plates (i.e., equivalent T-stub in mode (1) led to moment-rotation response characterized by large hysteretic loops; conversely, selecting thicker end-plates (i.e., equivalent T-stub in modes (2) and (3) led to concentrated plasticization in bolts and to low energy dissipation capacity. Hence, the thickness of end-plate can be selected with within the range 1/2 - 2/3 the bolt diameter;
- The revised ductility criterion is effective to enforce ductile failure mode (i.e., mode 1). However, the ductility of the joints is impaired by the failure of fillet welds;
- The fracture initiation in the fillet welds between the beam flange and the end-plate occurs prior to completion of the cyclic loading for the joints with the thinner end-plates and for the cases with compact beam section with large bolt horizontal pitch. These results suggest that even if FEP joints are used for gravity load resisting systems, it is necessary to design the welds with adequate overstrength with respect to the ultimate resistance of the thinner connected plate. Hence, the use of full penetration welds is advisable to guarantee adequate rotation capacity of connections designed to exhibit failure mode 1 per bolt row;
- The joints with the smaller diameter of the bolts and the thicker end-plates experience severe post-capping degradation, indicating that the mechanical model with perfectly plastic behaviour given by EN 1993-1-8 (CEN 2005) can be non-conservative;
- Increasing the number of bolt rows is beneficial both in terms of strength and rotation capacity under cyclic actions, due to increased internal force redistribution capacity;
- In the elastic range and up to low rotational demand values (i.e., smaller than 5 mrad), the most of FEP joints behave as semi-rigid, while at higher rotational demand the stiffness degradation becomes significant and the joints tend to behave as pinned;
- In terms of strength, the best performance under cyclic bending is recognized for the joints designed to exhibit failure mode 2 per bolt row, which minimize the plastic strain demand into the welds and do not exhibit their premature failure. In addition, these joints show good correspondence with predicted resistance at θ = 4%;
- Further investigation based on experimental tests is advisable to validate seismic design guidelines for FEP joints.

References

AISC (2016a), AISC 341-16 - Seismic provisions for structural steel buildings, Chicago, IL, USA.

AISC (2016b), ANSI/AISC 358-16 - Prequalified connections for special and intermediate steel moment frames for seismic applications, Chicago, IL, USA.

AISC (2016c), ANSI/AISC 360-16 - Specification for structural steel buildings, Chicago, IL, USA.

Aribert, J., Braham, M. and Lachal, A. (2004), "Testing of "simple" joints and their characterization for structural analysis", *J. Constr. Steel Res.*, **60**(3-5), 659-681.

Boorse, M. (1999), "Evaluation of the inelastic rotation capability of flush end-plate moment connections", M.Sc. Thesis; Virginia Polytechnic Institute and State University, Blacksburg, VA, USA.

Borgsmiller, J.T. and Murray, T.M. (1995), "Simplified method for design of moment end-plate connections", Report No. CE/VPI-ST 95/19, Blacksburg, VA, USA.

Broderick, B.M. and Thomson, A.W. (2002), "The response of flush end-plate joints under earthquake loading", *J. Constr. Struct. Res.*, **58**(9), 1161-1175.

Cassiano, D., D'Aniello, M., Rebelo, C., Landolfo, R. and Silva, L.S. (2016), "Influence of seismic design rules on the robustness of steel moment resisting frames", *Steel Compos. Struct., Int. J.*, **21**(3), 479-500.

Cassiano, D., D'Aniello, M. and Rebelo, C. (2017), "Parametric finite element analyses on flush end-plate joints under column removal", *J. Constr. Steel Res.*, **137**, 77-92.

CEN (2004), EN 1998-1 - Eurocode 8: Design of structures for earthquake resistance - Part 1: General rules, seismic actions and rules for buildings, Brussels, Belgium.

CEN (2005), EN 1993-1-8 - Eurocode 3 - Design of steel structures - Part 1-8: Design of joints, Brussels, Belgium.

Chi, W.M., Kanvinde, A.M. and Deierlein, G.G. (2006), "Prediction of ductile fracture in steel connections using SMCS criterion", *J. Struct. Eng.*, **132**(2), 171-181.

D'Aniello, M., Cassiano, D. and Landolfo, R. (2016), "Monotonic and cyclic inelastic tensile response of European preloadable gr10.9 bolt assemblies", *J. Constr. Steel Res.*, **124**, 77-90.

D'Aniello, M., Tartaglia, R., Costanzo, S. and Landolfo, R. (2017a), "Seismic design of extended stiffened end-plate joints in the framework of Eurocodes", *J. Constr. Steel Res.*, **128**, 512-527.

D'Aniello, M., Cassiano, D. and Landolfo, R. (2017b), "Simplified criteria for finite element modelling of European preloadable bolts", *Steel Compos. Struct., Int. J.*, **24**(6), 643-658.

Dassault (2013), Abaqus 6.13 - Abaqus Analysis User's Manual, Dassault SystèmesSimulia Corp.

Dusicka, P., Itani, A.M. and Buckle, I.G. (2007), "Cyclic response of steel plates under large inelastic strains", *J. Constr. Steel Res.*, **63**(2), 156-164.

El-Tawil, S., Vidarsson, E., Mikesell, T. and Kunnath, S.K. (1999), "Inelastic behaviour and design of steel panel zones", *J. Struct. Eng.*, **125**(2), 183-193.

Fang, C., Izzuddin, B.A., Elghazouli, A.Y. and Nethercot, D.A. (2013), "Robustness of multi-storey car parks under localised fire—towards practical design recommendations", *J. Constr. Steel Res.*, **90**, 193-208.

Fang C., Izzuddin B.A., Obiala R., Elghazouli, A.Y. and Nethercot, D.A. (2012), "Robustness of multi-storey car parks under vehicle fire", *J. Constr. Steel Res.*, **75**, 72-84.

Gioncu, V., Mosoarca, M. and Anastasiadis, A. (2014), "Local ductility of steel elements under near-field earthquake loading", *J. Constr. Steel Res.*, **101**, 33-52.

Girão Coelho, A.M. and Bijlaard, F. (2007), "Experimental behaviour of high strength steel end-plate connections", *J. Constr. Steel Res.*, **63**(9), 1228-1240.

Girão Coelho, A.M., da Silva, L.S. and Bijlaard, F. (2004), "Characterisation of the nonlinear behaviour of single bolted T-Stub connections", Connections in Steel Structures V.

Hancock, J.W. and Mackenzie, A.C. (1976), "On the mechanics of ductile failure in high-strength steel subjected to multi-axial stress-states", *J. Mech. Phys. Solids*, **24**(3), 147-160.

ISO (2009), EN ISO 2560 – Welding consumables. Covered electrodes for manual metal arc welding of non-alloy and fine grain steels.

Kuhlmann, U., Rölle, L., Jaspart, J.P., Demonceau, J.F., Vassart, O. and Weynand, K. (2009), "Robust structures by joint ductility - Final report", Research Fund for Coal and Steel.

Lamarche, C.P. and Tremblay, R. (2011), "Seismically induced cyclic buckling of steel columns including residual-stress and strain-rate effects", *J. Constr. Steel Res.*, **67**(9), 1401-1410.

Myers, A.T., Kanvinde, A.M. and Deierlein, G.G. (2010), "Calibration of the SMCS Criterion for Ductile Fracture in Steels: Specimen Size Dependence and Parameter Assessment", *J. Eng. Mech.*, **136**(11), 1401-1410.

Pavlovic, M., Heistermann, C., Veljkovic, M., Pak, D., Feldmann, M., Rebelo, C. and Silva, L.S. (2015), "Connections in towers for wind converters, part I: Evaluation of down-scaled experiments", *J. Constr. Steel Res.*, **115**, 445-457.

Da Silva, L.S., Lima, L., Vellasco, P. and Andrade, S. (2004), "Behaviour of flush end-plate beam to column joints under bending and axial force", *Steel Compos. Struct., Int. J.*, **4**(2), 77-94.

Srouji, R., Murray, T.M. and Kukreti, A.R. (1983), "Yield-line analysis of end-plate connections with bolt force predictions", Report No. FSEL/MBMA 8305, University of Oklahoma.

Tartaglia, R. and D'Aniello, M. (2017), "Nonlinear performance of extended stiffened end plate bolted beam-to-column joints subjected to column removal", *Open Civil Eng. J.*, **11**(1), 369-383.

Tartaglia, R., D'Aniello, M., Rassati, G.A., Swanson, J.A. and Landolfo, R. (2018), "Full strength extended stiffened end-plate joints: AISC vs recent European design criteria", *Eng. Struct.*, **159**, 155-171.

Wang, W., Fang, C., Qin, X., Chen, Y. and Li, L. (2016), "Performance of practical beam-to-SHS column connections against progressive collapse", *Eng. Struct.*, **106**, 332-347.

Yu, H., Burgess, I., Davison, J. and Planck, R. (2011), "Experimental and numerical investigations of the behaviour of flush end plate connections at elevated temperatures", *J. Constr. Eng.*, **137**(1), 80-87.

Zangouie, A.R. and Deylami, A. (2013), "Influence of beam flange thickness on seismic performance of flange plate connections", *Proceedings of the 13th East Asia-Pacific Conference on Structural Engineering and Construction* (*EASEC-13*), Sapporo, Japan, September.

CC